Digital Discovery

ROYAL SOCIETY OF CHEMISTRY

PAPER

View Article Online
View Journal

Cite this: DOI: 10.1039/d5dd00580a

ALBATROSS: a robotised system for high-throughput electrolyte screening *via* automated electrolyte formulation, coin-cell fabrication, and electrochemical evaluation

Hyun-Gi Lee,†[a] Jaekyeong Han,†[a] Minjun Kwon,[a] Hyeonuk Kwon,[b] Jooha Park,[c] Hoe Jin Hah[c] and Dong-Hwa Seo *[ab]

As battery technologies advance toward higher stability and energy density, the need for extensive cell-level testing across various component configurations becomes critical. To evaluate performance and understand the operating principles of batteries at the laboratory scale, the fabrication and evaluation of coin cells are essential processes. However, the conventional coin-cell assembly and testing processes require significant time and labor from researchers, posing challenges to high-throughput screening research. In this study, we introduce an Automated Li-ion BAttery Testing RObot SyStem (ALBATROSS), an automated system capable of electrolyte formulation, coin-cell assembly, and electrochemical evaluation. The system, integrated within an argon-filled glovebox, enables fully automated assembly and testing of up to 48 cells without researcher intervention. By incorporating a custom-designed robot gripper and 3D-printed structures optimized for precise cell handling, ALBATROSS achieved high assembly reproducibility, yielding a relative standard deviation (RSD) of 1.3% in discharge capacity and 6% in electrochemical impedance spectroscopy (EIS) measurements of bulk resistance for Li||NCM811 half-cells. Owing to its high reproducibility and automation capability, ALBATROSS allows for the acquisition of high-quality coin-cell datasets, which are expected to accelerate the development of next-generation electrolytes.

Received 23rd December 2025
Accepted 14th March 2026

DOI: 10.1039/d5dd00580a

rsc.li/digitaldiscovery

Introduction

Liquid electrolytes are one of the key components that govern the operation of lithium-ion batteries (LIBs). The liquid electrolytes serve as the medium for ion transport and govern high-rate capability, energy efficiency, the formation of interfacial layers such as the solid electrolyte interphase (SEI), and the thermal and chemical stability of the cell. To improve these properties, various types of electrolytes have been developed, and a wide range of salts, solvents, and additives have been created and utilized. It is anticipated that future electrolyte development will require careful selection and optimal combination of various salts, solvents, and additives.[1,2] Therefore, an efficient method for evaluating diverse electrolytes is needed, and this is typically done by assembling and testing coin cells, one of the smallest types of battery. However, assembling and testing a large number of coin cells requires significant time and labor from researchers, posing a challenge.

To overcome the limited availability of experimental data, robotics-based autonomous laboratories have recently gained significant attention.[3–6] In the field of liquid electrolytes, various automated platforms for electrolyte formulation and screening have been actively developed.[7–12] Among these efforts, several automated coin-cell assembly systems utilizing robotics within an argon-filled glovebox have been reported, including AutoBass,[13,14] Poseidon,[15] and ODACell.[16,17] These systems are designed to assemble numerous cells using pre-loaded cell components with minimal human intervention. Reportedly, AutoBass can assemble up to 64 cells at a rate of approximately one cell every 7 minutes, Poseidon assembles one cell approximately every 5 minutes (the maximum number of cells that can be assembled simultaneously was not specified), and ODACell can assemble up to 40 cells at a rate of approximately one cell every 2.5 minutes. Notably, both AutoBass and Poseidon are limited to the assembly process; subsequent electrochemical evaluations for LIBs such as cycling test must be performed manually by the researcher. ODACell extends this functionality by automating both cell assembly and cycling test. ODACell was later upgraded to increase the number of cycling channels from

[a]Department of Materials Science and Engineering, Korea Advanced Institute of Science and Technology (KAIST), Daejeon, 34141, Republic of Korea. E-mail: dseo@kaist.ac.kr
[b]Graduate School of Green Growth and Sustainability, Korea Advanced Institute of Science and Technology (KAIST), Daejeon, 34141, Republic of Korea
[c]LG Energy Solution, Seoul, 07796, Republic of Korea
† These authors contributed equally: Hyun-Gi Lee and Jaekyeong Han.

16 to 56. However, reported relative standard deviation (RSD) values were 3.46% for 57 cells in AutoBass, 3.2% for 11 cells in Poseidon, and 1.98% for 80 cells in ODACell. Because cycling tests are time-consuming, acquiring a large, high-quality dataset requires considerable time and effort. Therefore, to overcome this bottleneck, an automated system with highly reproducible coin-cell assembly and a large number of cycling channels is required to enable more efficient data acquisition.

On the other hand, while charge–discharge curves provide essential information about the overall performance of a cell, they offer limited insight into the underlying degradation mechanisms. Electrochemical impedance spectroscopy (EIS), which enables the interpretation of bulk resistance, charge-transfer resistance, and SEI resistance, can serve as a complementary analytical tool for analyzing cell degradation.[18,19] Despite its diagnostic utility, obtaining EIS data for multiple cells is often limited because frequent manual intervention is required to conduct both cycling and impedance measuring steps. As a result, EIS is usually performed only on a small number of selected cells, either immediately after formation or after long-term cycling for lifetime assessment. To overcome these constraints, the development of an integrated system capable of automatically performing both charge–discharge cycling test and EIS analysis is important. Such a system would enable the acquisition of comprehensive electrochemical and impedance data across a large number of cells with minimal manual effort, thereby facilitating a deeper understanding of the underlying principles of cell degradation.

The aforementioned challenges can be addressed through the following key strategies:

(1) Systematic formulation of electrolytes with various combinations and ratios of salts, solvents, and additives.

(2) Automated assembly of a large number of cells without human intervention.

(3) Full automation of charge–discharge tests and EIS measurements for the assembled cells.

In this work, to implement these strategies, we developed Automated Li-ion BAttery Testing RObot SyStem (ALBATROSS), an integrated, fully automated platform capable of assembling and evaluating up to 48 cells without researcher involvement (Fig. 1). ALBATROSS performs electrolyte formulation (Tables S1 and S2), coin-cell assembly (Fig. S1–S5), charge–discharge cycling, and EIS measurements (Fig. S6 and S7) within an argon-filled glovebox environment. The platform incorporates 48 cycling channels and 2 EIS channels, enabling the efficient collection of both electrochemical and impedance data. The system is capable of formulating an electrolyte, assembling a coin cell, and initiating a cycling test within 4 minutes. The system also demonstrated high assembly repeatability, yielding an RSD of less than 1.3% in discharge capacity and 6% in EIS

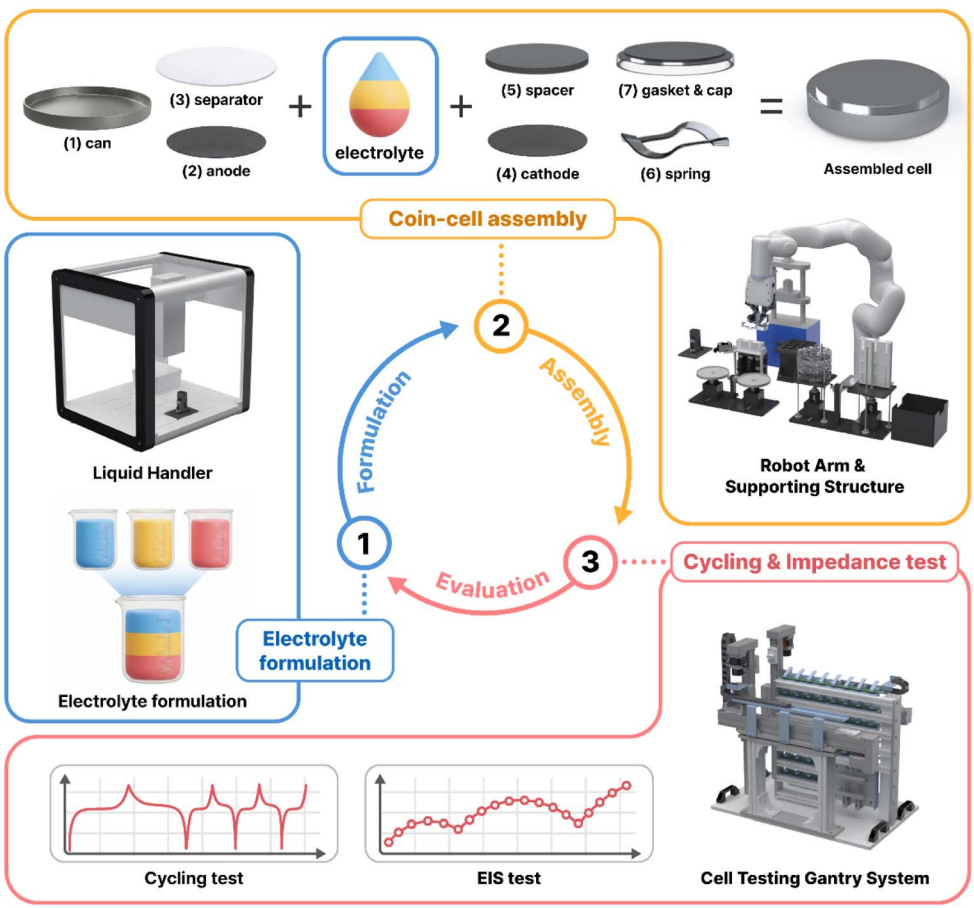

Fig. 1 Illustration of ALBATROSS flow: (1) formulating liquid electrolyte, (2) assembling coin cells using formulated electrolyte, (3) evaluating assembled cells.

measurements of bulk resistance. To achieve this level of automation, a variety of 3D-printed structures (Fig. S2 and S3) and a custom-designed robot gripper (Fig. S4 and S5) were developed and integrated into the platform. With ALBATROSS, extensive cycling and impedance datasets can be obtained across diverse electrolyte composition spaces, providing insights into the fundamental roles of electrolytes and accelerating electrolyte development. Moreover, this platform is expected to extend beyond liquid electrolyte screening to address a broader range of challenges, including the optimization of formation protocols for SEI design,[20] and the exploration of fast charge–discharge protocols.[21]

Methods

Devices and materials

The automated system for electrolyte formulation, cell assembly, and evaluation was constructed using a 6-axis robot arm (xArm6, UFactory), a liquid handler (OT-2, Opentrons), an automated coin-cell crimper (MSK-160E, MTI), customized with an elevated vertical axis to ensure unobstructed access by the robot arm. Additional actuating and motion components including stepper motors (C-42STM03, Misumi) and linear actuators (12LF-12F-27 and 12LF-17F-40, Mightyzap) were utilized. System control and synchronization were managed using a programmable logic controller (PLC; NX102-9000, Omron) (Fig. S8 and S9). Custom structural parts were designed in CAD and fabricated using a 3D printer (A15CR, Cubicon) with PLA filament or from aluminum using CNC machining when necessary. Cycling test equipments (Neware, CT-4008T-5V50mA-164) and impedance measurement devices (Biologics, SP-150e) were installed inside the glovebox.

For the reproducibility tests, 2032-type coin-cell cases (MTI) were used as cell enclosures. The cathode consisted of a 12.5 mm diameter NCM811 electrode (Wellcos), and the anode was a 16 mm diameter, 0.1 mm thick lithium metal foil (Honjo). A 19 mm diameter glass fiber separator (Whatman) was employed, and each cell was filled with 70 μL of electrolyte composed of 1 M $LiPF_6$ in EC : EMC (3 : 7 vol%) with 2 wt% VC additives (EnChem). All components were handled within the argon-filled glovebox to prevent moisture or oxygen contamination.

Electrolyte formulation

In this system, electrolyte formulation was tested using the liquid handler. To prepare electrolytes with various compositions, concentrated salt solutions were diluted with pure solvents to the desired concentrations (Tables S1 and S2). For solvents such as ethylene carbonate (EC), which are solid at room temperature, a temperature-control module inside the liquid handler was used to maintain the solvent at 60 °C prior to dispensing. To eliminate the risk of cross-contamination, a new pipette tip was used for every solution transfer and mixing step. During aspiration, any excess solution adhering to the pipette tip was removed by touching the tip to the vial entrance. The solutions were then mixed using the automated micropipette, which performed 20 repetitive mixing strokes over a total duration of 3 minutes.

Electrochemical analysis

To evaluate the reproducibility of cell cycling, two formation cycles followed by 50 main cycles were conducted for all assembled cells. The formation cycles were conducted within a voltage range of 3.0–4.3 V at a 0.1 C-rate, using a constant current–constant voltage (CCCV) charging and a constant current (CC) discharging mode. Subsequently, the main cycles were performed within a range of 3.0–4.2 V at a 1 C-rate using CC charging and discharging mode. For comparative analysis, 40 cells manually assembled by a researcher and 80 cells assembled using ALBATROSS were tested under identical conditions.

To verify the reproducibility of EIS measurements, an additional set of 40 newly assembled cells was evaluated using the automated system. Each cell underwent a 12-hours rest period, followed by two formation cycles at 0.1 C-rate between 3.0–4.3 V, and then two charge–discharge cycles at 0.5, 1, 2, and 3 C-rates within the 3.0–4.2 V range. EIS measurements were performed after a 12-hours rest period and the completion of two cycles at 1, 2, and 3 C-rates, following a 30-minutes rest period,[22,23] over a frequency range of 200 kHz to 0.1 Hz. If two cells enter the EIS-measurement waiting status simultaneously, the second cell initiates its EIS measurement immediately after the first cell completes its measurement.

Results and discussion

ALBATROSS integrates a liquid handler, a robot arm, potentiostats, and EIS modules within a four-port glovebox, enabling fully automated electrolyte formulation, coin-cell assembly, and electrochemical evaluation without human intervention. The system assembled coin cells with a success rate of 100% (120 out of 120 cells) through minor adjustments to the robot motion (SI Section 6, Fig. S10–S13). A single operation, which included electrolyte formulation, cell assembly, and initiation of the cycling test, required approximately 4 minutes, allowing the system to process 48 cells in roughly 200 minutes. Assuming that the electrochemical cycling procedure requires approximately six days, the platform is capable of generating data for up to 240 cells per month.

In addition to the capability for high-throughput data generation, a critical aspect of any automated system is the achievement of high reproducibility.[24] High reproducibility serves as an indicator that, by leveraging the precise and consistent operation of mechanical components, experimental errors and variations that may arise from manual handling by researchers can be minimized, thereby enabling the acquisition of high-quality data. Coin-cell assembly and evaluation involve the handling of diverse cell components and the management of charge–discharge processes for multiple cells, making considerable effort necessary to ensure reproducibility. In the following sections, we describe the strategies implemented to

secure high-quality data and present the corresponding test results.

The developed ALBATROSS is composed of three main automated modules: (I) electrolyte formulation, (II) coin-cell assembly using the formulated electrolyte, and (III) electrochemical evaluation of the assembled cells (Fig. 2 and 3). The electrolyte formulation module utilizes a liquid handler to enable automated mixing and dispensing of electrolyte components. The cell assembly module is operated by a robot arm, while the electrochemical testing module is constructed based on gantry systems integrated with potentiostat and impedance measurement devices. Unlike conventional glovebox-integrated automation systems, which often employ compact robots due to limited internal space, ALBATROSS adopts a 6-axis robot arm with a wide working range (700 mm). This design choice was made to accommodate the simultaneous assembly of a large number of cells and the handling of various devices and associated waste, which requires broader operational range. However, employing a 6-axis robot arm within the confined space of a glovebox makes challenges related to its limited maneuverability. To mitigate this, the system incorporates two key strategies: (1) the implementation of supporting structures that spatially arrange the cell components within the robot's effective working area (Fig. S2 and S3), and (2) the development of a custom gripper capable of handling multiple types of components with a simple mechanical structure (Fig. S4 and S5). A detailed discussion follows in subsequent sections.

Coin-cell assembly

The coin-cell assembly and evaluation processes were conducted using the robot arm. To enable the automated assembly and evaluation of 48 cells simultaneously, the robot arm was designed with a gripper capable of accommodating both a parallel gripper and a vacuum gripper (Fig. S4). The vacuum gripper was used to transfer the coin-cell components, including the can, anode, and separator, after which the liquid dispenser precisely dispensed the electrolyte into the cell. Subsequently, the cathode, spacer, spring, and cap were transferred and then assembled using an automated crimper, completing the coin-cell assembly. Since transferring the spring was difficult with the vacuum gripper, the parallel gripper was utilized for this task.

The system was installed within a glovebox, making robot-coordinate calibration challenging and necessitating simplification of the calibration process. Simply arranging the components at fixed equal distances would make future recalibration difficult, particularly considering that there are 48 sets of 7 different components, totaling 336 components. Such an arrangement could not only complicate coordinate recalibration but also impede the robot arm's accessibility. To facilitate reliable handling of various components and simplify coordinate calibration, supporting structures were fabricated to supply all components to the robot arm at fixed positions (Fig. 2, S1 and S2). Using rotary and stackable structures, cell components pre-arranged in sets of 12 were consistently positioned to enhance robot accessibility and repeatability. This configuration ensured that components were always transferred to the same location, which is critical as precise component placement strongly influences subsequent cell performance. It also reduced the number of robot's calibration points from 336 to 8, dramatically improving recalibration efficiency, which are critical issues for systems operating inside a glovebox. The use of these supporting structures substantially improved the reproducibility of the assembled cells.

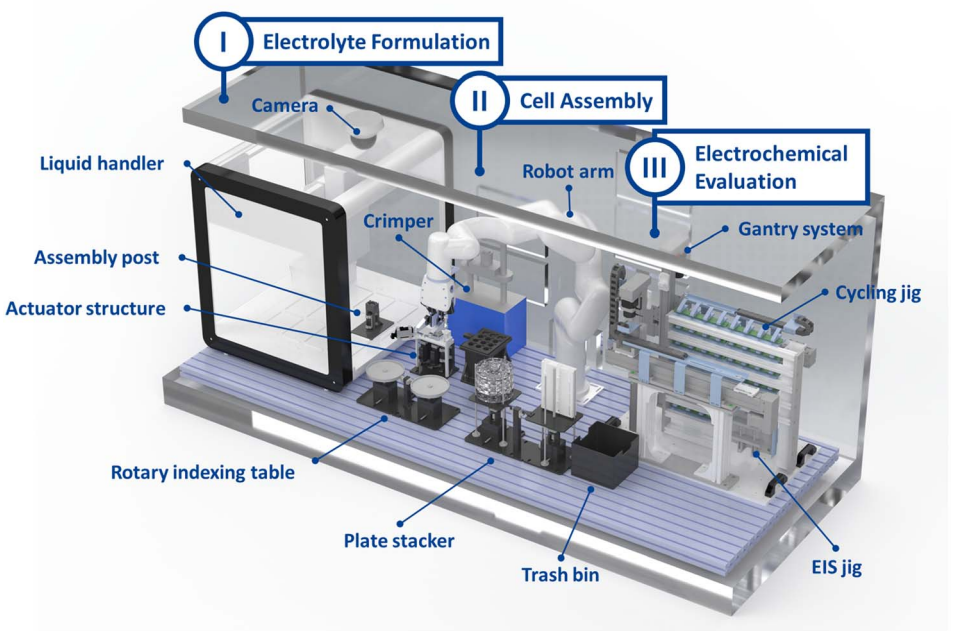

Fig. 2 Schematic illustration of ALBATROSS setup. (I) Electrolyte formulation and dispense part using the liquid handler. (II) Coin-cell assembly part using the robot arm. (III) Coin-cell electrochemical evaluation part using two gantry systems, potentiostats and impedance measurement instruments.

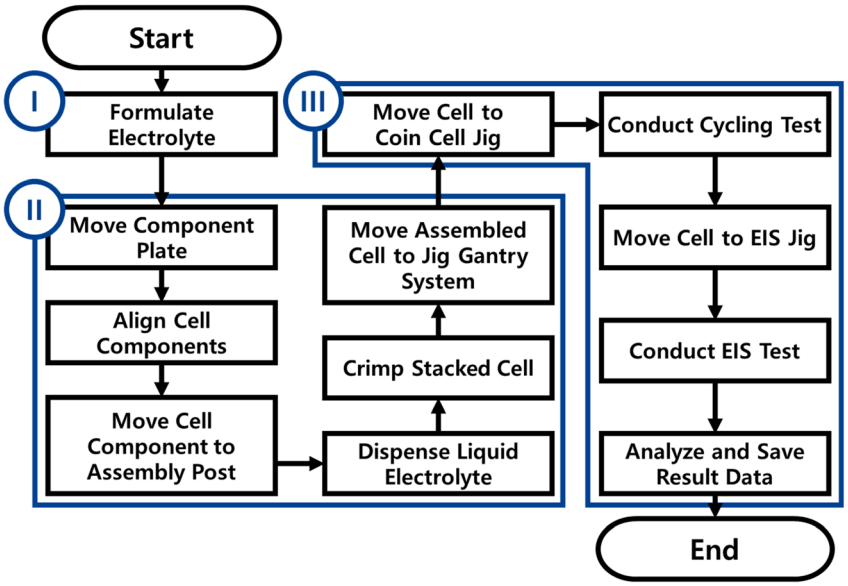

Fig. 3 Flowchart of ALBATROSS. (I) Electrolyte formulation, (II) coin-cell assembly, (III) coin-cell electrochemical evaluation.

The system assembles 48 cells automatically by utilizing four component plates, each containing 12 parts. Positioning these plates for robotic handling posed challenges because plates occupy a relatively considerable volume, require unobstructed access for robotic gripping, and must be handled within the confined space of a glovebox, where maneuverability is inherently limited. As a result, the plate-storage structure, referred to here as the plate stacker, had to fulfill two competing requirements: occupying minimal space while simultaneously elevating the plates to a height that enables easy robotic access and providing sufficient mechanical support to prevent plate tilting or collapse. As is common in specialized automation systems, no commercially available structure could satisfy these constraints. Therefore, we disassembled a cartesian robot and repurposed the robot components to design a custom storage mechanism. The resulting structures consistently positioned each plate at an elevated and robot-accessible location (Fig. 2, S1 and S3). This customized solution effectively mitigated the accessibility limitations imposed by the glovebox environment and reduced the likelihood of operational failures due to spatial interference or unstable component positioning. Consequently, the plate stacker enhances the overall operational reliability of the automated assembly workflow.

Cell evaluation

After assembly process, the assembled cells were then transported from the crimper to the cycling gantry system, which consisted of two gantries designed for automated cycling and EIS evaluation (Fig. 2, S6 and S7). The automated cycling and EIS system was configured with 48 potentiostat channels and 2 EIS channels. Directly transferring the coin cells from the robot arm to all 48 potentiostat channels or 2 EIS channels is challenging, as it requires simultaneous control of the jig opening and cell placement. To address this, two gantry systems were employed to receive the coin cells from the robot arm at the fixed position and reliably transfer them to vacant cycling channels. This process operates independently of the robot arm, substantially enhancing the efficiency of the workflow from assembly to evaluation.

As a result, the entire process, from electrolyte formulation to electrochemical evaluation, was fully automated without human intervention. Moreover, the system enabled EIS measurements to be automatically performed during cycling, not only for a subset of cells but for all 48 cells, allowing detailed monitoring of degradation behavior and the acquisition of large amounts of experimental data.

Reproducibility test

To evaluate the performance of the completed system, 80 cells were assembled using ALBATROSS and another 40 cells were manually assembled by a researcher under the identical electrolyte composition. All cells underwent cycling tests with the same protocol. For reproducibility analysis, the average, standard deviation, and relative standard deviation (RSD) of the formation cycle and 50th of the main cycle data were calculated. The RSD serves as an indicator of system reproducibility, with values near 1% considered to represent excellent consistency.

$$\overline{x} = \frac{\sum x}{n}, s = \sqrt{\frac{\sum (x - \overline{x})}{n - 1}}, \widehat{c_v} = \frac{s}{\overline{x}}$$

($\bar{x}$: mean of sample, n: the number of samples, s: sample standard deviation, $\widehat{c_v}$: coefficient of variance (CV) or relative standard deviation (RSD))

The 40 cells manually assembled by the researcher exhibited an RSD of 2.375% in the formation cycle and 2.310% in the 50th cycle. Similarly, the 80 cells assembled using ALBATROSS showed an RSD of 1.292% in the formation cycle and 1.365% in the 50th cycle, which are comparable to the manually

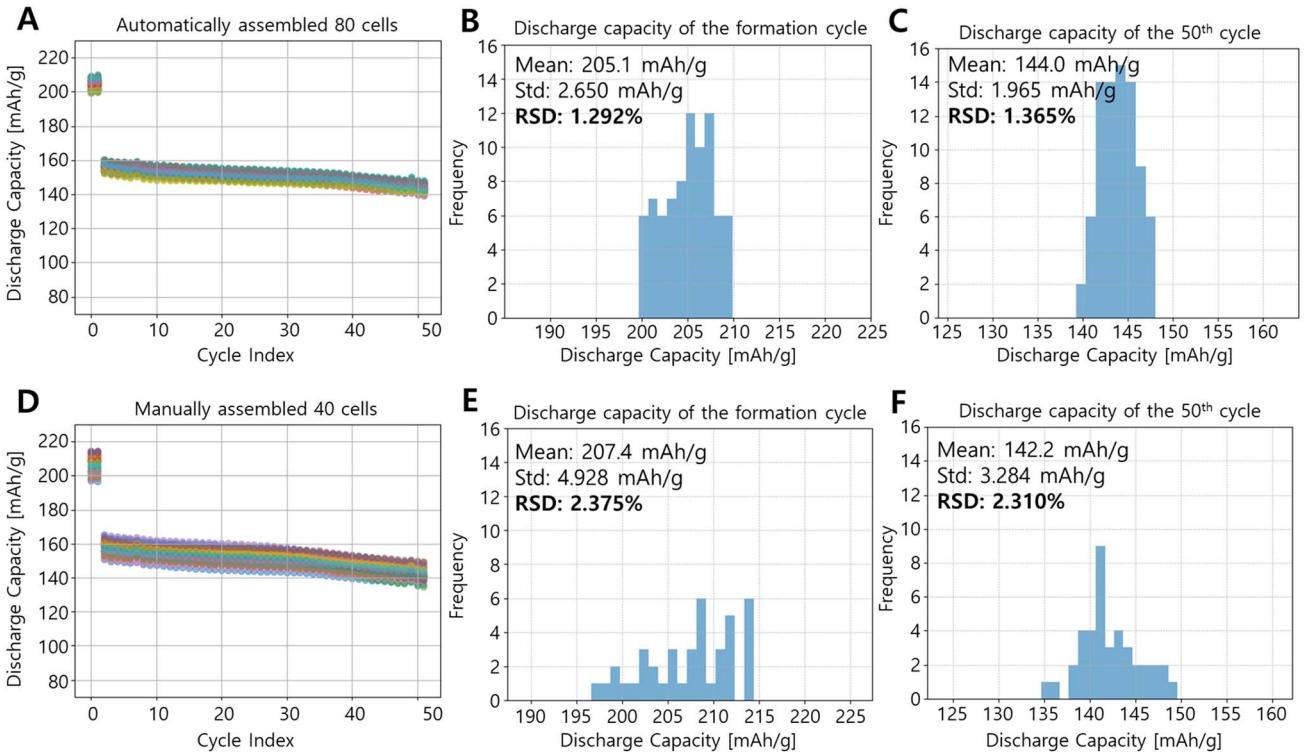

Fig. 4 Discharge-capacity profiles and reproducibility results for the formation and the 50th cycle of 80 cells assembled by ALBATROSS and 40 cells assembled by a human researcher. (A–C) Cycle test results of 80 cells assembled by ALBATROSS and (D–F) results of 40 cells assembled manually. (A and D) Discharge-capacity profiles, (B and E) histogram of discharge capacity of the formation cycle, and (C and F) histogram of the 50th cycle.

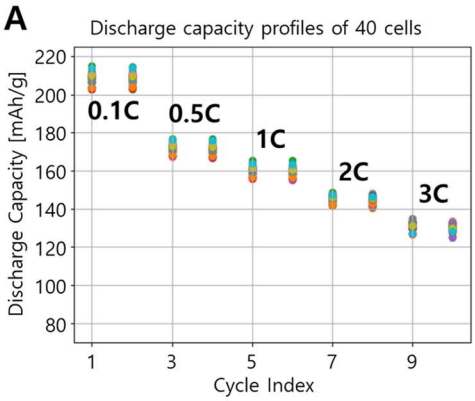

B

C-rate	Mean [mAh/g]	Std. [mAh/g]	RSD
0.1C	208.1	2.916	1.40%
0.5C	171.1	2.555	1.49%
1C	159.5	2.440	1.53%
2C	144.5	2.018	1.40%
3C	130.1	2.124	1.63%

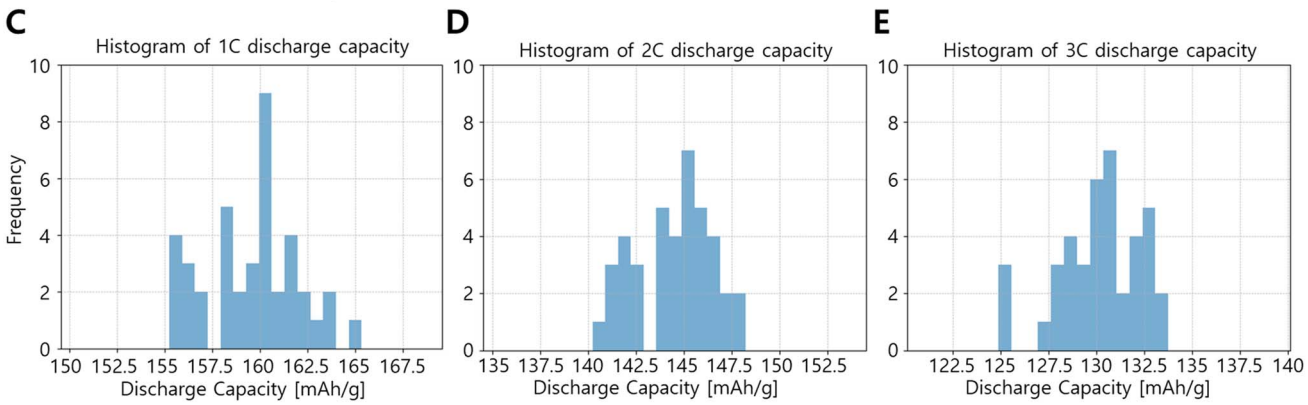

Fig. 5 Cycling results of 40 cells used for EIS evaluation. (A and B) Discharge capacity of 40 cells cycled at 0.1 C, 0.5 C, 1 C, 2 C, and 3 C. (C–E) Histograms of discharge capacity distributions at 1 C, 2 C, and 3 C.

assembled results (Fig. 4). These results demonstrate that ALBATROSS achieved a level of reproducibility better than that of an experienced researcher, confirming the reliability of the automated assembly process.

Automated impedance measurement

For EIS evaluation, 40 newly assembled cells were tested after a 12-hours rest period followed by two formation cycles at 0.1 C and subsequent cycling at 0.5 C, 1 C, 2 C, and 3 C. The capacity reproducibility exhibited similar trends to those observed in the previous tests (Fig. 5). Subsequent EIS measurements were then conducted for the same cells after a 12-hours rest and after cycling at 1 C, 2 C, and 3 C (Fig. 6 and S14–S17). The EIS data were analyzed based on an equivalent circuit model composed of one ohmic resistance (R_1, R_{bulk}), two parallel RC elements representing the SEI resistance (R_2, R_{SEI}), and charge-transfer resistance (R_3, R_{CT}), and a Warburg impedance element (Fig. 6A). Ideally, the diffusion process is represented by a Warburg impedance; however, in the present electrode configuration, the Nyquist plots did not exhibit the characteristic 45-degree slope in the low-frequency region (Fig. S14). Therefore, the Warburg element was replaced with a constant phase element (CPE) to account for non-ideal diffusion behavior.[25–27]

Despite the inherently high sensitivity of impedance spectroscopy, the reproducibility of the EIS data was acceptable; however, some variations among cells were observed. These variations in EIS measurements are considered to be partially attributable to differences in rest period and temperature fluctuation within the glovebox (Fig. S18–S21). Considering that the primary objective of ALBATROSS is to acquire EIS datasets for a wide range of electrolyte systems, that no existing platform currently enables systematic acquisition of EIS and ambient temperature data, and that resistance changes induced by electrolyte variation are substantially larger than the observed cell-to-cell variability, ALBATROSS is considered suitable for high-throughput screening applications.

Future direction for high-throughput electrolyte discovery

Despite the development of ALBATROSS, the design space for electrolytes remains extremely large. In fact, the primary bottleneck in electrolyte evaluation is not the fabrication of the electrolyte or cell assembly, but the long-term evaluation of cells. To efficiently identify promising electrolytes, three key strategies are required: (1) defining an appropriate variable domain, (2) conducting design of experiments through artificial intelligence models, and (3) developing accelerated charge–discharge protocols for rapid cell evaluation. Accordingly, a feasible approach involves selecting candidate composition domains through first-principles calculations, followed by rapid exploration using AI-driven design of experiments models based on experimental data obtained from the automated system. Furthermore, developing reliable AI models capable of

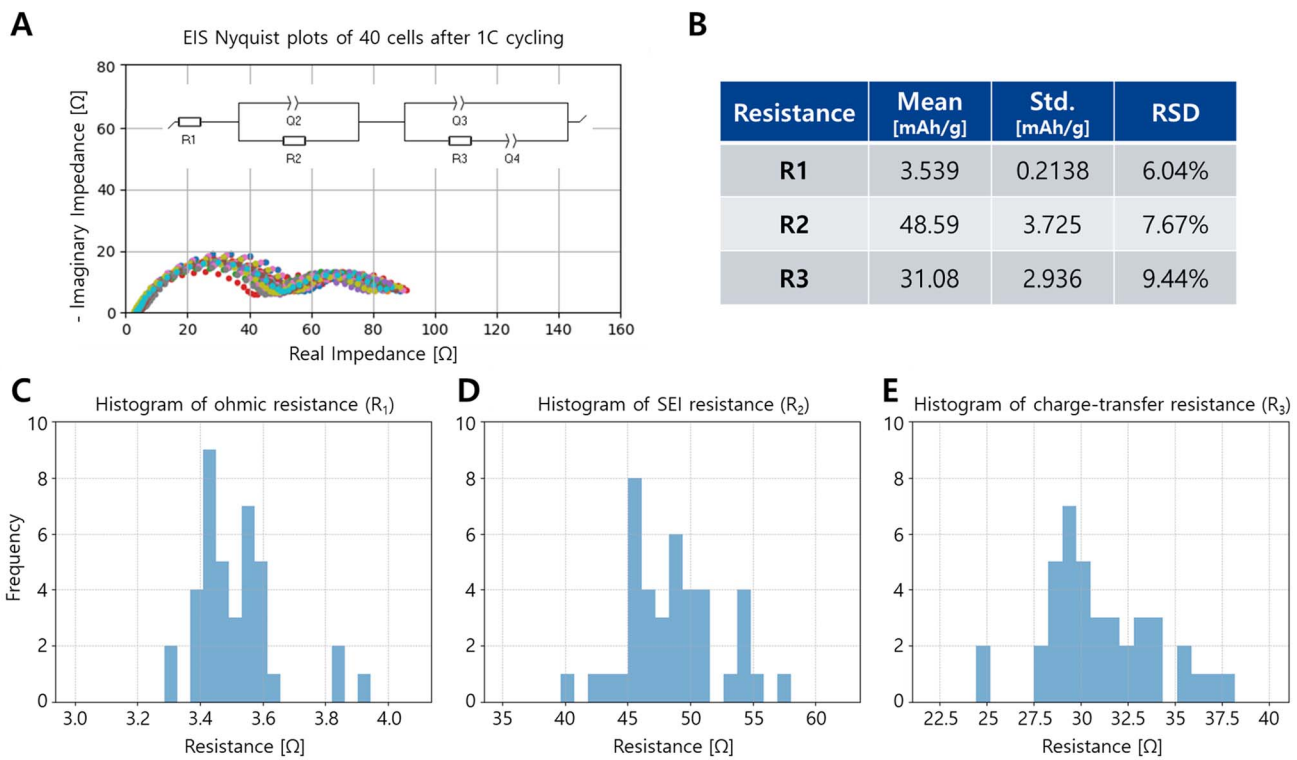

Resistance	Mean [mAh/g]	Std. [mAh/g]	RSD
R1	3.539	0.2138	6.04%
R2	48.59	3.725	7.67%
R3	31.08	2.936	9.44%

Fig. 6 EIS results of 40 cells after 1 C cycling. (A) Schematic of the equivalent circuit and Nyquist plots for 40 cells and (B) mean, standard deviation, and RSD results of fitted resistance values. (C–E) Histograms of resistance distribution for different resistance components (R_1, R_2, and R_3).

predicting long-term cycle life from short-term charge–discharge tests[28–30] and EIS measurements[19,31,32] is essential.

Conclusion

In this study, we introduced ALBATROSS, an automated platform for high-throughput electrolyte screening. The system integrates three major modules: electrolyte formulation and dispensing, coin-cell assembly, and electrochemical evaluation. This configuration enables fully automated cell fabrication and evaluation of up to 48 cells without manual intervention. To ensure reliable operation, a custom-designed gripper and supporting structures were implemented to align and handle cell components, resulting in highly reproducible cell capacities. In addition, the system can perform EIS measurements on all 48 cells during cycling, providing comprehensive impedance data that could reveal the underlying mechanisms of cell degradation. We anticipate that the high-quality data generated by ALBATROSS will accelerate the discovery of electrolytes, particularly for challenging battery systems such as lithium-metal, lithium-sulfur, and sodium-ion systems.

Author contributions

Hyun-Gi Lee contributed to investigation, hardware, software, validation, writing – original draft, writing – review & editing, and visualization. Jaekyeong Han contributed to investigation, formal analysis, software, and writing – review & editing. Minjun Kwon contributed to hardware and software. Hyeonuk Kwon contributed to data curation, software, and validation. Jooha Park contributed to resources, methodology, and writing – review & editing. Hoe Jin Hah contributed to resources, methodology, and writing – review & editing. Dong-Hwa Seo contributed to conceptualization, resources, methodology, supervision, and writing – review & editing, and project administration.

Conflicts of interest

There are no conflicts to declare.

Data availability

All the codes, program files and videos for ALBATROSS can be found at https://github.com/Hyun-Gi/ALBATROSS with DOI: https://doi.org/10.5281/zenodo.18959775.

Supplementary information (SI) is available. See DOI: https://doi.org/10.1039/d5dd00580a.

Acknowledgements

This research was supported by the LG Energy Solution.

References

1 S. C. Kim, J. Wang, R. Xu, P. Zhang, Y. Chen, Z. Huang, Y. Yang, Z. Yu, S. T. Oyakhire, W. Zhang, L. C. Greenburg, M. S. Kim, D. T. Boyle, P. Sayavong, Y. Ye, J. Qin, Z. Bao and Y. Cui, High-entropy electrolytes for practical lithium metal batteries, *Nat. Energy*, 2023, **8**(8), 814–826.
2 J. Xu, J. Zhang, T. P. Pollard, Q. Li, S. Tan, S. Hou, H. Wan, F. Chen, H. He, E. Hu, K. Xu, X. Q. Yang, O. Borodin and C. Wang, Electrolyte design for Li-ion batteries under extreme operating conditions, *Nature*, 2023, **614**(7949), 694–700.
3 B. Burger, P. M. Maffettone, V. V. Gusev, C. M. Aitchison, Y. Bai, X. Wang, X. Li, B. M. Alston, B. Li, R. Clowes, N. Rankin, B. Harris, R. S. Sprick and A. I. Cooper, A mobile robotic chemist, *Nature*, 2020, **583**(7815), 237–241.
4 N. J. Szymanski, B. Rendy, Y. Fei, R. E. Kumar, T. He, D. Milsted, M. J. McDermott, M. Gallant, E. D. Cubuk, A. Merchant, H. Kim, A. Jain, C. J. Bartel, K. Persson, Y. Zeng and G. Ceder, An autonomous laboratory for the accelerated synthesis of novel materials, *Nature*, 2023, **624**(7990), 86–91.
5 J. Chen, S. R. Cross, L. J. Miara, J.-J. Cho, Y. Wang and W. Sun, Navigating phase diagram complexity to guide robotic inorganic materials synthesis, *Nat. Synth.*, 2024, **3**(5), 606–614.
6 Z. Zhang, Z. Ren, C. W. Hsu, W. Chen, Z. W. Hong, C. F. Lee, A. Penn, H. Xu, D. J. Zheng, S. Miao, Y. Huang, Y. Gao, W. Chen, H. Smith, Y. Niu, Y. Tian, Y. R. Lu, Y. C. Shao, S. Li, H. T. Wang, I. I. Abate, P. Agrawal, Y. Shao-Horn and J. Li, A multimodal robotic platform for multi-element electrocatalyst discovery, *Nature*, 2025, **647**(8089), 390–396.
7 S. Matsuda, K. Nishioka and S. Nakanishi, High-throughput combinatorial screening of multi-component electrolyte additives to improve the performance of Li metal secondary batteries, *Sci. Rep.*, 2019, **9**(1), 6211.
8 S. Matsuda, G. Lambard and K. Sodeyama, Data-driven automated robotic experiments accelerate discovery of multi-component electrolyte for rechargeable Li–O_2 batteries, *Cell Rep. Phys. Sci.*, 2022, **3**(4), 100832.
9 A. Dave, J. Mitchell, K. Kandasamy, H. Wang, S. Burke, B. Paria, B. Póczos, J. Whitacre and V. Viswanathan, Autonomous Discovery of Battery Electrolytes with Robotic Experimentation and Machine Learning, *Cell Rep. Phys. Sci.*, 2020, **1**(12), 100264.
10 A. Dave, J. Mitchell, S. Burke, H. Lin, J. Whitacre and V. Viswanathan, Autonomous optimization of non-aqueous Li-ion battery electrolytes *via* robotic experimentation and machine learning coupling, *Nat. Commun.*, 2022, **13**(1), 5454.
11 M. Ramezani, P. Nandi, P. A. De La Fuente-Moreno and M. Beidaghi, BRINE: a cost-effective electrochemical self-driving laboratory for accelerated discovery of high-performance electrolytes, *Digital Discov.*, 2026, **5**(1), 397–406.
12 G. Tom, S. P. Schmid, S. G. Baird, Y. Cao, K. Darvish, H. Hao, S. Lo, S. Pablo-Garcia, E. M. Rajaonson, M. Skreta, N. Yoshikawa, S. Corapi, G. D. Akkoc, F. Strieth-Kalthoff, M. Seifrid and A. Aspuru-Guzik, Self-Driving Laboratories for Chemistry and Materials Science, *Chem. Rev.*, 2024, **124**(16), 9633–9732.
13 B. Zhang, L. Merker, A. Sanin and H. S. Stein, Robotic cell assembly to accelerate battery research, *Digital Discov.*, 2022, **1**(6), 755–762.

14 B. Zhang, L. Merker, M. Vogler, F. Rahmanian and S. S. Helge, Apples to apples: shift from mass ratio to additive molecules per electrode area to optimize Li-ion batteries, *Digital Discov.*, 2024, **3**(7), 1342–1349.

15 P. H. Svensson, P. Yushmanov, A. Tot, L. Kloo, E. Berg and K. Edström, Robotised screening and characterisation for accelerated discovery of novel Lithium-ion battery electrolytes: Building a platform and proof of principle studies, *Chem.–Eng. J.*, 2023, **455**, 140955.

16 J. T. Yik, L. Zhang, J. Sjölund, X. Hou, P. H. Svensson, K. Edström and E. J. Berg, Automated electrolyte formulation and coin cell assembly for high-throughput lithium-ion battery research, *Digital Discov.*, 2023, **2**(3), 799–808.

17 J. T. Yik, C. Hvarfner, J. Sjölund, E. J. Berg and L. Zhang, Accelerating aqueous electrolyte design with automated full-cell battery experimentation and Bayesian optimization, *Cell Rep. Phys. Sci.*, 2025, **6**(5), 102548.

18 H.-M. Cho, Y. J. Park, J.-W. Yeon and H.-C. Shin, In-Depth Investigation on Two- and Three-Electrode Impedance Measurements in Terms of the Effect of the Counter Electrode, *Electron. Mater. Lett.*, 2009, **5**(4), 169–178.

19 Y. Zhang, Q. Tang, Y. Zhang, J. Wang, U. Stimming and A. A. Lee, Identifying degradation patterns of lithium ion batteries from impedance spectroscopy using machine learning, *Nat. Commun.*, 2020, **11**(1), 1706.

20 X. Cui, S. D. Kang, S. Wang, J. A. Rose, H. Lian, A. Geslin, S. B. Torrisi, M. Z. Bazant, S. Sun and W. C. Chueh, Data-driven analysis of battery formation reveals the role of electrode utilization in extending cycle life, *Joule*, 2024, **8**(11), 3072–3087.

21 D. T. Boyle, Y. Li, A. Pei, R. A. Vila, Z. Zhang, P. Sayavong, M. S. Kim, W. Huang, H. Wang, Y. Liu, R. Xu, R. Sinclair, J. Qin, Z. Bao and Y. Cui, Resolving Current-Dependent Regimes of Electroplating Mechanisms for Fast Charging Lithium Metal Anodes, *Nano Lett.*, 2022, **22**(20), 8224–8232.

22 A. De Angelis, P. Carbone, A. Moschitta, M. Crescentini, R. Ramilli and P. Traverso, in *A fast and simple broadband EIS measurement system for Li-Ion batteries, 24th IMEKO TC4 International Symposium and 22nd International Workshop on ADC and DAC Modelling and Testing*, International Measurement Confederation (IMEKO), 2020, pp. 157–161.

23 L. Mattia, B. Ospina Agudelo, H. Beiranvand, M. Liserre and W. Zamboni, Lithium-ion battery impedance as a battery temperature indicator, *J. Energy Storage*, 2025, **132**, 117879.

24 A. I. Cooper, P. Courtney, K. Darvish, M. Eckhoff, H. Fakhruldeen, A. Gabrielli, A. Garg, S. Haddadin, K. Harada, J. Hein, M. Hübner, D. Knobbe, G. Pizzuto, F. Shkurti, R. Shrestha, K. Thurow, R. Vescovi, B. Vogel-Heuser, Á. Wolf, N. Yoshikawa, Y. Zeng, Z. Zhou and H. Zwirnmann, Accelerating discovery in natural science laboratories with AI and robotics: Perspectives and challenges, *Sci. Robot.*, 2025, **10**(106), eadv7932.

25 M. Oldenburger, B. Bedürftig, A. Gruhle, F. Grimsmann, E. Richter, R. Findeisen and A. Hintennach, Investigation of the low frequency Warburg impedance of Li-ion cells by frequency domain measurements, *J. Energy Storage*, 2019, **21**, 272–280.

26 N. Meddings, M. Heinrich, F. Overney, J.-S. Lee, V. Ruiz, E. Napolitano, S. Seitz, G. Hinds, R. Raccichini, M. Gaberšček and J. Park, Application of electrochemical impedance spectroscopy to commercial Li-ion cells: A review, *J. Power Sources*, 2020, **480**, 228742.

27 P. Vadhva, J. Hu, M. J. Johnson, R. Stocker, M. Braglia, D. J. L. Brett and A. J. E. Rettie, Electrochemical Impedance Spectroscopy for All-Solid-State Batteries: Theory, Methods and Future Outlook, *ChemElectroChem*, 2021, **8**(11), 1930–1947.

28 K. A. Severson, P. M. Attia, N. Jin, N. Perkins, B. Jiang, Z. Yang, M. H. Chen, M. Aykol, P. K. Herring, D. Fraggedakis, M. Z. Bazant, S. J. Harris, W. C. Chueh and R. D. Braatz, Data-driven prediction of battery cycle life before capacity degradation, *Nat. Energy*, 2019, **4**(5), 383–391.

29 F. Wang, Z. Zhai, Z. Zhao, Y. Di and X. Chen, Physics-informed neural network for lithium-ion battery degradation stable modeling and prognosis, *Nat. Commun.*, 2024, **15**(1), 4332.

30 I. Kim, H. Kim, S. An, J. Oh, M. Kim and J. W. Choi, Degradation path prediction of lithium-ion batteries under dynamic operating sequences, *Energy Environ. Sci.*, 2025, **18**(8), 3784–3794.

31 P. K. Jones, U. Stimming and A. A. Lee, Impedance-based forecasting of lithium-ion battery performance amid uneven usage, *Nat. Commun.*, 2022, **13**(1), 4806.

32 S. Zhang, W. Yuan, Y. Wang, S. Cheng and J. Wang, Early-stage lifetime prediction for lithium-ion batteries: Linear regression – ensemble learning hybrid model based on impedance spectroscopy geometry, *J. Power Sources*, 2024, **617**, 235153.